JIKaP

Journal of Indigenous Knowledge and Practice

2025, Vol. 1, No. 1, pp. 83-95

Article History: Received: 2 December 2025; Reviewed: 3 April 2025; Revised: 17 May 2025; Accepted: 7 June 2025

Impact of Aerosol on Atmospheric Ozone over Langtang National Park, Nepal

Prakash M. Shrestha[1,2*], Suresh P. Gupta[1], Krishna B. Rai[1], Usha Joshi[1], Narayan P. Chapagain[3], Indra B. Karki[1] and Khem N. Poudyal[4]

[1]*Department of Physics, Patan Multiple Campus, TU, Nepal*

[2]*Central Department of Physics, TU, Nepal*

[3]*Department of Physics, Amrit Campus, TU, Nepal*

[4]*Department of Applied Sciences and Chemical Engineering, Pulchowk Campus, TU, Nepal*

Abstract

This paper reports the impact of aerosols on atmospheric ozone over Langtang National Park. The daily ground-based data of AOD and TOC are received from the Aerosol Robotic Network of NASA for a period of one-year 2018. The daily, monthly and seasonal variations of AOD and TOC are analyzed. The annual average of AOD for visible light are found 0.039 ± 0.037, 0.056 ± 0.049 and 0.064 ± 0.056 respectively. For infrared, the annual average of AOD are found 0.027 ± 0.026 and 0.031 ± 0.030 respectively. For ultraviolet, annual average of AOD are found 0.074 ± 0.064 and 0.079 ± 0.069 respectively. During the study period, the annual average of TOC is found 265 ± 2 DU. There is positive impact of AOD on TOC with moderate correlation coefficient. The result of this work is beneficial for the further analysis of AOD, TOC and their impact at different places.

Keywords: Aerosol optical depth, infrared, total ozone column, ultra violet, visible light

Introduction

Aerosols are minute solid or liquid particles that float in the atmosphere, including substances like dust, smoke, soot, sea salt, and pollutants from industry. These particles originate from natural sources such as volcanic eruptions and desert dust and human activities, like burning fossil fuels and agricultural practices. Sun radiates 4 x 10^{26} J of energy per second. Out of total energy 1367 W/m^2 (solar constant) (Duffie & Beckman, 2013) incidents on outer layer of the atmosphere when Earth is at mean

*Corresponding Author's email: prakashman4516@gmail.com

ISSN: 3102-0216

distance of 1.49×10^8 km from the Sun. The Solar radiation interacts with large particle of the atmosphere such as water droplets, dust and aerosol. According to Beer Lambert's law, the solar radiation decreases exponentially with extinction coefficient (k) and optical air mass (m) in the atmosphere (Lothian, 1963; Shrestha et al., 2024). The extinction of solar radiation is the sum of extinction due to gas mixture, water vapor, ozone, aerosol and Rayleigh scattering. Extinction coefficient due to aerosol is called aerosol optical depth (AOD).

The sun emits electromagnetic waves with large wavelength (λ) range. About 50 percent of the radiation is under the infrared ($\lambda > 700$ nm) region, 40 percent falls in visible region ($400 \text{ nm} < \lambda < 700$ nm) and 10 percent falls in the ultraviolet (UV) region ($100 \text{ nm} < \lambda < 400$ nm) (Chapagain, 2016). The atmospheric ozone is a form of the element oxygen with the chemical formula O_3. In 1930 S. Chapman, a British scientist, proposed a theory of the formation of ozone and its decomposition in the stratosphere known as the Chapman mechanism. Ozone protects earth's surface from ultraviolet radiation by absorbing radiation below 300 nm (Volz & Kley, 1988). Approximately 90 percent of the ozone in the atmosphere is concentrated in the stratosphere, between from 15 to 50 km above the Earth's surface. The UV-C (wavelength range 100 nm to 280 nm) is completely absorbed by the ozone layer and only five percent of UV-B (wavelength range 280 nm to 315 nm) reaches the Earth's surface, while nearly the 95 percentage of UV-A (wavelength range 315 nm to 400 nm) can to penetrate the atmospheric layers. The UV radiation has a number of effects on human health. However, shorter wavelength UV radiation is less able to penetrate through the skin.

Figure 1

Map of Langtang

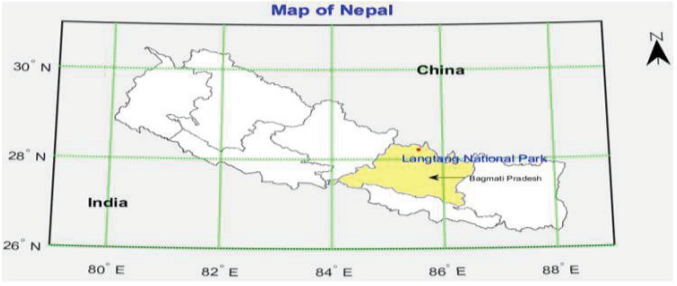

Source: Survey Department, Gov. of Nepal, 2020

Langtang National Park (28.21° N, 85.56° E and altitude 3862 m a.s.l.) is first Himalayan national park and covers an area of 1,710 sq. km of land. The national park lies in Nuwakot, Sindhupalchowk and Rasuwa districts in the central Himalayan region of Nepal (Bhuju et al., 2007). Gosai kunda, Surya kunda, Dudh kunda, Bhairav kunda, and Parvati kunda lie on this national park.

The National Parke has a wide variety of climatic zones ranging from subtropical to alpine. The days are warm and sunny during April, May, October, and November. The annual average of Angstrom exponential (α), Angstrom turbidity coefficient (β) and Linke turbidity factor (L_T) are found 1.04 ± 0.29, 0.03± 0.02 and 2.5 ± 0.6 respectively on 2018 (Shrestha et al., 2022). The location of the national park is shown in figure 1.

Literature Review

Aerosols are suspended solid and liquid particles with sizes ranging from 1 nm to 10 μm. Both natural and anthropogenic aerosols influence the solar radiation in three ways: directly by affecting the scattering and absorption of solar radiation, indirectly by altering cloud microphysics and lifetime, and semi-directly by affecting cloud formation or evaporation (Ramanathan & Carmichael, 2008). One of anthropogenic aerosols, black carbon, is emitted by vehicles and kilns and produces the greenhouse effect. It melts ice laying on mountain. Vehicles also emit particulate matter, including fine particles like PM10 and PM2.5, which are small enough to be inhaled deeply into the lungs. These airborne particles can penetrate the respiratory system, leading to a range of health problems such as asthma, bronchitis, reduced lung function, and other serious respiratory illnesses in humans. Long-term exposure can also contribute to cardiovascular diseases and increase the risk of premature death (Putero et al., 2018). The atmospheric turbidity index plays an important role in air pollution studies, and research on it is valuable for further identifying, assessing, and analyzing its impact on meteorological parameters in different locations with similar geographical conditions (Shrestha et al., 2023). Nepal is a land-locked south east mountainous Asian country with a large area of beautiful landscape. Within this small and beautiful setting, it possesses diversity in biosphere and variation of climate.

Nepal geographically lies within sun-belt (latitude 15° N to 35° N). Annual solar isolation is 3.6 to 6.2 kWh/m^2/day with sunshine duration of 300 days in Nepal

(Shrestha et al., 2003). In 2016, 538.6 TJ energy is consumed in which traditional fuel is 73 percent, commercial fuel is 25 percent and renewable energy is 2 percent (MoF, 2018). In Nepal, 4,37,614 automobiles were registered during the fiscal year BS 2074/075. This significant rise in vehicles registrations had a number of consequences, such as worsened air pollution, more traffic jams, and a burden on public transportation and road infrastructure (DTM, 2075). Earthquakes cause significant crustal deformation, leading to dust generation, landslides, soil and rock exposure, and forest fires. These effects release aerosols (particulate matter, black carbon, etc.) into the atmosphere. Aerosols play a key role in the atmosphere and act as catalysts for ozone-depleting reactions, especially in the troposphere and modify temperature and humidity, which influence ozone formation and breakdown. Regions downwind of aerosol sources may experience temporary or localized ozone depletion (Shrestha et al., 2022). A large amount of foreign currency is used to export petroleum products. Due to petroleum fuel-based vehicles, air pollution increases day by day. So, the study of air pollution together with the impact of aerosols on atmospheric Ozone is very important and is needed at this time.

Research Methods

The daily ground-based data of spectral aerosol optical depth (AOD) and total ozone column (TOC) are received from Aerosol Robotic Network (AERONET) of NASA for a period of one year 2018 (NASA. 2000). The daily satellite based data of TOC are received from NASA website (NASA, 2001).

Open source software Python 3.7 is used on Jupyter note of Anaconda program to analyze data and to plot graphs. Quartiles (Q_1, Q_2, Q_3), skewness (γ_1) and kurtosis (γ_2) are used as statistical tool to analyze the nature of distribution of time series data (Stephens & Spiegel, 1998).

$$\gamma_1 = \frac{\mu_3}{\sqrt{\mu_2^3}} \quad \ldots\ldots\ldots\ldots\ldots\ldots \quad (1)$$

$$\gamma_2 = \frac{\mu_4}{\mu_2^2} - 3 \quad \ldots\ldots\ldots\ldots\ldots\ldots \quad (2)$$

Here μ_2, μ_3 and μ_4 are second, third and fourth moment about mean respectively. Coefficient of variance (CV) is used to check variability of data.

$$CV = \frac{\sigma}{\bar{x}} x100 \quad \ldots\ldots\ldots\ldots\ldots \quad (3)$$

Standard error (SE) is used as error bar in graph. Data presented in forms of 'mean ($\bar{x}$) ± standard deviation (σ)'.

$$SE = \frac{\sigma}{\sqrt{n}} \qquad \ldots\ldots\ldots\ldots\ldots\ldots\ldots \quad (4)$$

Here n is the number of data. Fourier series is used to analysis seasonal variation of time series data (Shrestha et al., 2020).

$$y_s = a_0 + a_1 \cos\left(\frac{2\pi}{365} n_d\right) + b_1 \sin\left(\frac{2\pi}{365} n_d\right) \quad \ldots\ldots\ldots\ldots\ldots \quad (5)$$

Here n_d is day number of year. It is 1 for first January and 365 for 31 December. Correlation coefficient (r) is used to find relation between two data x and y. Its value ranges from -1 to +1.

$$r = \frac{\sum_{i=1}^{n}(x_i - \bar{x})(y_i - \bar{y})}{\sqrt{\sum_{i=1}^{n}(x_i - \bar{x})^2}\sqrt{\sum_{i=1}^{n}(y_i - \bar{y})^2}} \qquad \ldots\ldots\ldots\ldots\ldots \quad (6)$$

Results and Discussion

The daily ground based data of aerosol optical depth (AOD) and total ozone column (TOC) are received from AERONET for the period of one year 2018. The daily satellite based data of total ozone column (TOC) are received from the NASA website. The skewness (γ_1) and kurtosis (γ_2) of daily data of AOD and TOC are calculated by using equations (1) and (2).

Variation of Aerosol Optical Depth (AOD)

Figure 2(a) and 2(b) show daily variation and box plot of aerosol optical depth (AOD). The maximum value of AOD for visible light having 675, 500 and 440 nm wavelengths are found to be 0.304, 0.323 and 0.358 respectively. For infrared with the wavelengths 1020 and 870 nm, the maximum values of AOD are found 0.272 and 0.283 respectively. For ultra violet corresponding to the wavelengths 380 and 340 nm, the maximum value of AOD are found 0.423 and 0.454 respectively. The minimum value of AOD for visible light (675, 500 and 440 nm wavelengths) are found 0.003, 0.008 and 0.008 respectively. For infrared (1020 and 870 nm wavelengths), the minimum value of AOD are found 0.003 and 0.002 respectively. For ultra violet (380 and 340 nm wavelengths), the minimum value of AOD are found 0.010 and 0.008 respectively. For easy convenience, the statistical parameters of AOD are shown in Table 1. The mean of AOD for wavelength 1020, 870, 675, 500, 440, 380 and 340 nm are 0.026, 0.030, 0.039, 0.057, 0.065, 0.074 and 0.079 respectively. The coefficient of variance (CV) for those

AOD are found 102, 100, 94, 87, 87, 86 and 87 respectively. CV of all AOD are greater than the 20 percentage. All AOD are scattered largely. The skewness (γ_1) of all AOD are positive. So the distribution of AOD is positively tailed. The kurtosis (γ_2) are greater than three. The distribution of AOD is Lepto kurtic (high peak). Figure 2(c) shows monthly variation AOD. All AOD are maximum in April. The maximum value of monthly average of AOD for wavelengths 1020, 870, 675, 500, 440, 380 and 340 nm are 0.064 ± 0.050, 0.075 ± 0.052, 0.097 ± 0.057, 0.135 ± 0.067 ,0.153 ± 0.074, 0.174 ± 0,082 and 0.188 ± 0.089 respectively. From this figure, the minimum value is found in August. The minimum value of monthly average of AOD are 0.008 ± 0.002, 0.009 ± 0.003, 0.011 ± 0.03, 0.020 ± 0.004, 0.025 ± 0.005, 0.032 ± 0.005 and 0.031 ± 0.008 respectively. Figure 2(d) shows seasonal variation of AOD. All AOD is maximum on spring and minimum on winter. The maximum value of seasonal average of AOD for wavelength 1020,870, 675,500,440,380 and 340 nm are 0.051 ± 0.038, 0.060 ± 0.040, 0.079 ± 0.047, 0.111 ± 0.060, 0.127 ± 0.068, 0.145 ± 0.077 and 0.156 ± 0.085 respectively. The minimum value of seasonal average of AOD are 0.017 ± 0.10, 0.019 ± 0.012, 0.026 ± 0.017, 0.037 ± 0.026, 0.041 ± 0.030, 0.045 ± 0.05 and 0.051 ± 0.038 respectively.

Figure 2

Variation of AOD (a) daily variation (b) box plot (c) monthly variation (d) seasonal variation

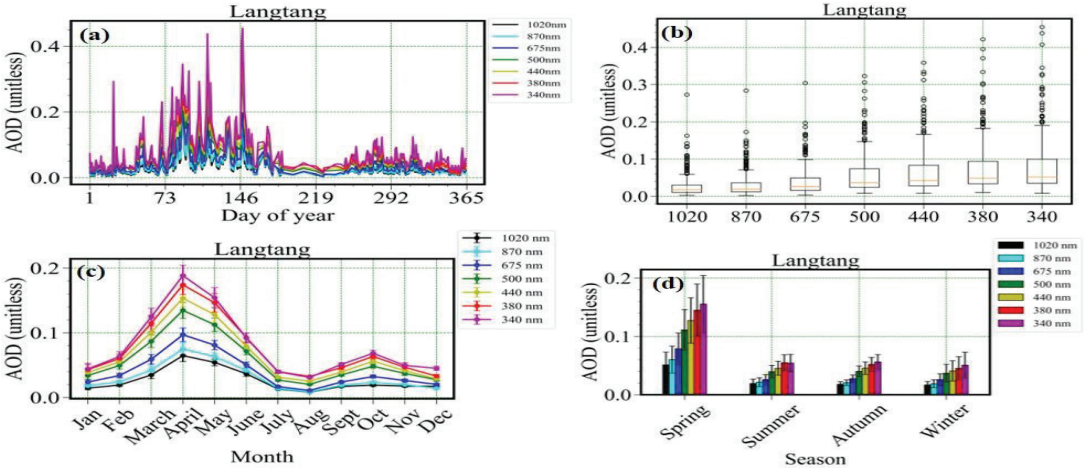

Table 1

Statistical Value of AOD

AOD	Maximum	Minimum	Q_1	Q_2	Q_3	γ_1	γ_2
1020 nm	0.272	0.002	0.011	0.019	0.030	3.72	22.31
870 nm	0.283	0.002	0.012	0.019	0.036	3.20	16.36
675 nm	0.304	0.003	0.016	0.026	0.049	2.58	9.62
500 nm	0.323	0.008	0.024	0.037	0.074	2.22	6.02
440 nm	0.358	0.008	0.028	0.042	0.083	2.19	5.78
380 nm	0.423	0.010	0.034	0.048	0.094	2.23	6.16
340 nm	0.454	0.008	0.035	0.052	0.100	2.29	6.52

After getting the daily data of AOD, it is fitted in Fourier series using equation (5). The offset (a_0) and amplitude of seasonal components ($\sqrt{a_1 + b_1}$) of AOD is shown in Table 2.

Table 2

Fourier Coefficient of AOD

AOD	a_0	a_1	b_1	$\sqrt{a_1 + b_1}$
1020 nm	0.026	-0.007	0.017	0.018
870 nm	0.030	-0.008	0.021	0.022
675 nm	0.039	-0.009	0.027	0.028
500 nm	0.057	-0.014	0.037	0.039
440 nm	0.065	-0.016	0.042	0.045
380 nm	0.074	-0.021	0.046	0.051
340 nm	0.089	-0.019	0.049	0.053

The annual average of AOD for wavelengths 675, 500,440,380 and 340 nm in Jomsom in 2012 are 0.0677 ± 0.0655, 0.1017 ± 0.0984, 0.1198 ± 0.1166, 0.1400 ± 0.1361 and 0.1560 ± 0.1513, respectively (Anton et al., 2011).

Variation of total ozone column (TOC)

Figure 3(a) and 3(b) show daily variation and histogram of total ozone column (TOC). Red line indicates ground based data and blue color indicates satellite based data of TOC. The maximum value of ground based data is 284 DU on 14 April and minimum 247 DU on 14 October. The root mean square deviation (RMSE) of satellite based data with ground based data is 13 DU. The first quartile (Q_1), second quartile (Q_2) and third quartile(Q_3) are 255, 265 and 277 DU respectively. The skewness (γ_1) and

kurtosis (γ_2) are found 0.02 and -1.30 respectively. Out of 365 days, 93 days has TOC between 260 DU to 270 DU. Figure 3(c) shows monthly variation TOC. The maximum value of TOC is 283 ± 1 DU on April and minimum value is 248 ± 1 DU on November respectively. The variation of TOC is large in February due to a large value of standard deviation 3 DU and less in November due to less standard deviation 1 DU. Figure 3(d) shows the seasonal variation of TOC. The maximum value of TOC is 280 ± 2 DU in spring whereas the minimum value is 254 ± 2 DU in autumn. The variation of TOC is large in winter due to a large value of standard deviation 2 DU and less variation is in summer due to a smaller value in standard deviation 1 DU.

The daily data of TOC is fitted in a Fourier series in equation (5) as shown in Figure 3(e). The offset (a_0) is 266 DU and the amplitude of seasonal components ($\sqrt{a_1 + b_1}$) is 16 DU. The annual average of TOC during 2004 to April 2016 in Kathmandu Valley was found 268 DU (Chapagain, 2016). The annual average of TOC in Jumla was found 271.84 ± 14.19 DU for 2008 to 2014 (Shrestha et al., 2021).

Figure 3

Variation of Total Ozone Column (TOC) (a) Daily Variation (b) Histogram (c) Monthly Variation (d) Seasonal Variation (e) Fourier Analysis

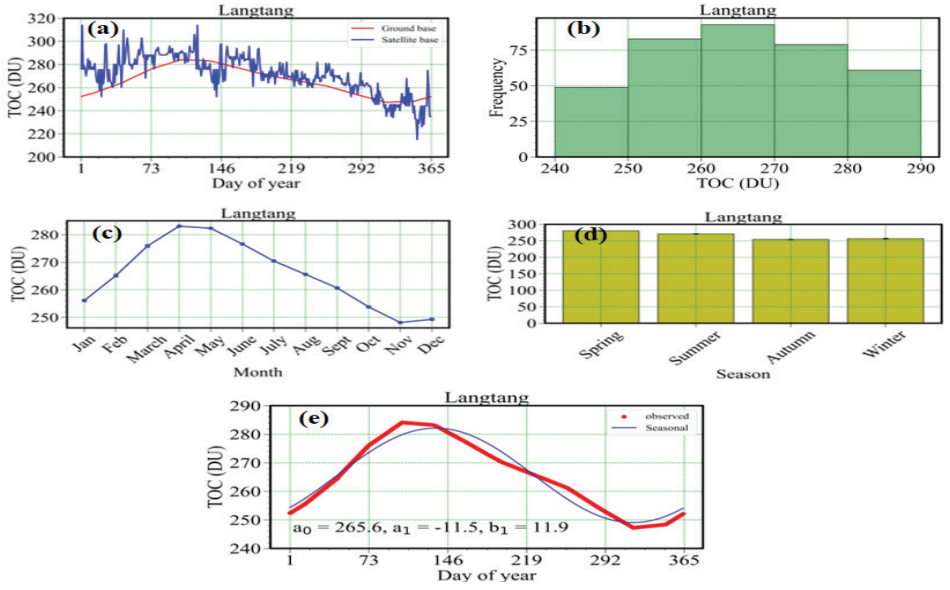

Over India from 2006 to 2010, lower tropospheric ozone showed that the highest concentrations were in the pre-summer monsoon season (May) and the lowest concentrations in the summer monsoon season (August) (Lu et al., 2018). Spatial-temporal distribution of ozone in 7 megacities of China such as Beijing, Chengdu and Hangzhou and others had the highest value of 160 μg m^{-3} during 2014 to 2016 (Gong et al., 2018) and this informs how ozone pollution has changed over time and across seven large cities.

Variation of TOC with AOD

The correlation coefficient of AOD and TOC is calculated by using equation (6). Figure 4(a) shows variation of AOD for 340 nm with TOC. The correlation coefficient of AOD for 340 nm is 0.55. There is positive effect of AOD for 340 nm on TOC. Figure 4(b) shows variation of AOD for 380 nm with TOC. The correlation coefficient of AOD for 380 nm is 0.56. There is positive effect of AOD for 380 nm on TOC. Figure 4(c) shows variation of AOD for 440 nm with TOC. The correlation coefficient of AOD for 440 nm is 0.57. There is positive effect of AOD for 440 nm on TOC. Figure 4(d) shows variation of AOD for 500 nm with TOC. The correlation coefficient of AOD for 500 nm is 0.56. There is positive effect of AOD for 500 nm on TOC. Figure 4(e) shows variation of AOD for 675 nm with TOC. The correlation coefficient of AOD for 675 nm is 0.53.

There is also positive effect of AOD for 675 nm on TOC. Figure 4(f) shows variation of AOD for 870 nm with TOC. The correlation coefficient of AOD for 870 nm is 0.52. There is positive effect of AOD for 870 nm on TOC. Figure 4(g) shows variation of AOD for 1020 nm with TOC. The correlation coefficient of AOD for 1020 nm is 0.48. There is positive effect of AOD for 1020 nm on TOC. This data shows a moderate positive relationship between aerosol levels (at 1020 nm) and ozone levels in the atmosphere. As aerosol levels go up, ozone levels also tend to rise.

Figure 4

Variation of TOC with AOD (a) 340 nm (b) 380 nm (c) 440 nm (d) 500 nm (e) 675 nm (f) 870 nm (g) 1020 nm

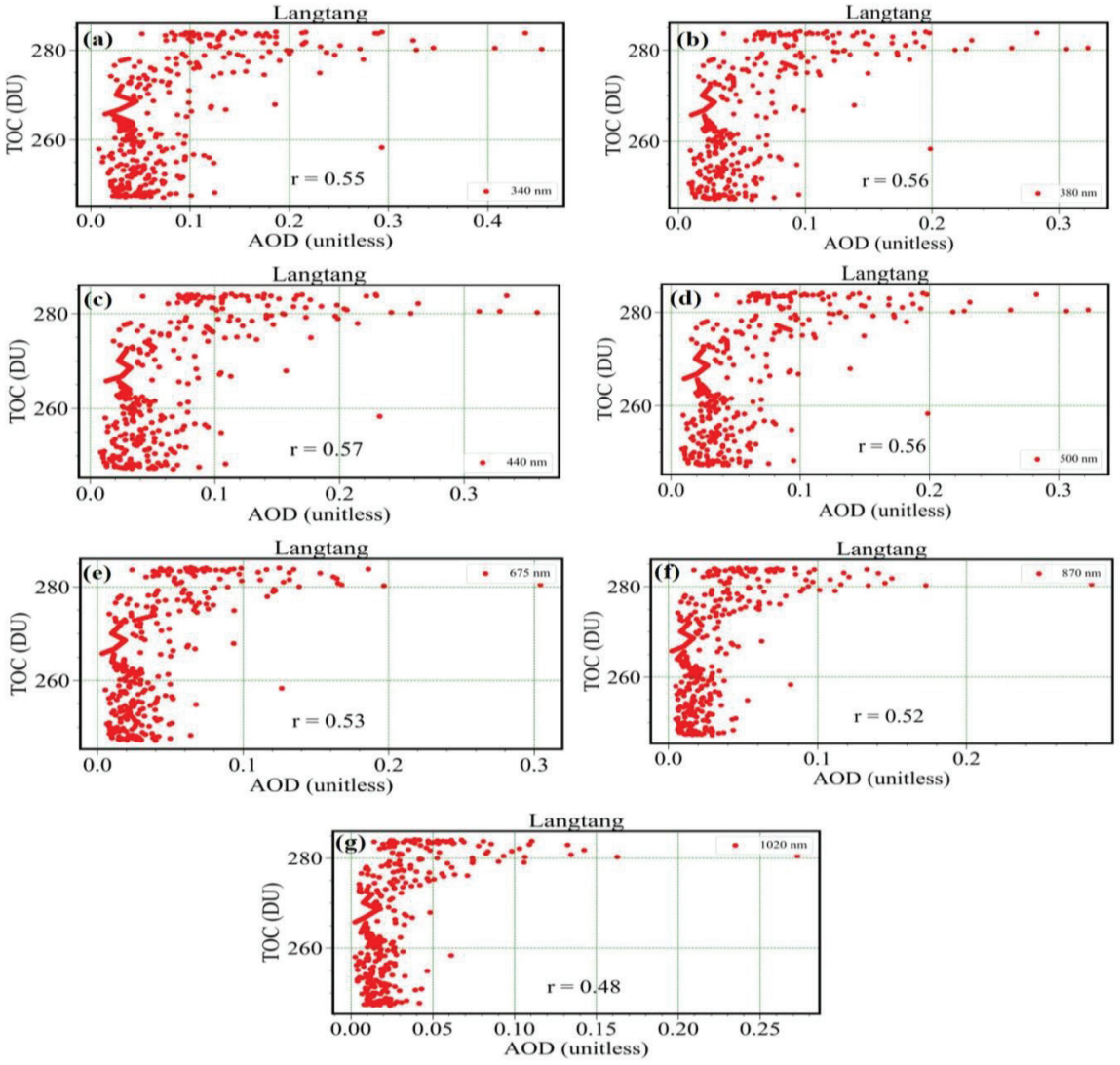

Conclusion and Implications

Aerosols, which include dust, smoke, soot, sea salt, and industrial pollutants, are tiny solid or liquid particles that float in the atmosphere. Both natural sources, such as volcanic eruptions and desert dust and human activities such as burning fossil fuels and farming, are the origins of these particles. For Langtang National Park with one year (2018) study period, the annual average of TOC is 265 ± 12 DU. The annual average of AOD for visible light (675, 500 and 440 nm) are found 0.039 ± 0.037, 0.056 ± 0.049 and 0.064 ± 0.056 respectively, for infrared (1020 and 870 nm), annual average of AOD are found 0.027 ± 0.026 and 0.031 ± 0.030 respectively. For ultraviolet (380 and 340 nm), an annual average of AOD are found 0.074 ± 0.064 and 0.079 ± 0.069 respectively. It highlights environmental risks such as ozone depletion and UV increase, underscores aerosols' role in Himalayan climate change, and calls for better air quality monitoring, pollution control, and awareness to protect ecosystems, health, tourism, and local livelihoods.

Conflict of Interest

The authors declare that there is no conflict of interest regarding publication of this article.

Acknowledgments

The authors would like to thank the faculty members of the Institute of Science and Technology (IoST), the Central Department of Physics (CDP), and the Department of Physics of the Patan Multiple Campus. The NASA for data and the Nepal Academy of Science and Technology (NAST) for PhD fellowship and are greatly appreciated by the authors. We would also like to thank the Association of Nepali Physicists in America (ANPA) and the Nepal Physical Society (NPS) for their assistance with the Python computer programming training.

References

Anton, M., Bortoli, D., Costa, M. J., Kulkarni, P. S., Domingues, A. F., Barriopedro, D., Serrano, A., & Silva, A. M. (2011). Temporal and spatial variabilities of total ozone column over Portugal. *Remote Sensing of Environment*, *115*(3), 855–863. 10.1016/j.rse.2010.11.013

Bhuju, U. R., Shakya, P. R., Basnet, T. B., & Shrestha, S. (2007). *Nepal Biodiversity Resource Book Protected Areas, Ramsar Sites, and World Heritage Sites*. ICIMOD UNEP.

Chapagain, N. P. (2016). Investigating temporal variability of total ozone column over Kathmandu using omi satellite obvservations. *JIST*, *21*(1), 140–147. 10.3126/jist.v21i1.16066

Department of Transport Management (DTM). (2075). *Register vehicles till fiscal year BS 2074/075.* Ministry of Physical Infrastructure and Transport, Government of Nepal.

Duffie, J. A., & Beckman, W. A. (2013). *Solar engineering of thermal processes*. John

Gong, X., Hong, S., & Jaffe, D. A. (2018). Ozone in China: Spatial Distribution and Leading Meteorological Factors Controlling O_3 in 16 Chinese Cities. *Aerosol and Air Quality Research*, 1*8,* 2287-2300. 10.4209/aaqr.2017.10.0368

https://aeronet.gsfc.nasa.gov/new_web/aerosols.html (Accessed on 20/12/2022)

Lothian, G. F. (1963). Beer's law and its use in analysis: A review. *Analyst*, *88*(1050), 678-685. 10.1039/AN9638800678

Lu, X., Zhang, L., Liu, X., Gao, M., Zhao, Y., & Shao, J. (2018). Lower tropospheric ozone over India and its linkage to the South Asian monsoon. *Atmospheric Chemistry Physics, 18*(5), 3101-3118.10.5194/acp-18-3101-2018

MoF. *Economic Survey 2018/019*. Ministry of Finance, Government of Nepal, 2018.

NASA. (2000). *Aeronet*. https://power.larc.nasa.gov/data-access-viewer/

NASA. (2001). *The power project.* https://power.larc.nasa.gov/data-access-viewer/ (Accessed on 10/01/2021)

Putero, D., Marinoni, A., Bonasoni, P., Calzolari, F., Rupakheti, M., & Cristofanelli, P. (2018). Black Carbon and Ozone Variability at the Kathmandu Valley and at the Southern Himalayas: A Comparison between a "Hot Spot" and a Downwind High-Altitude Site. *Aerosol and Air Quality Research, 18*(3), 623–635. https://doi.org/10.4209/aaqr.2017.04.0138

Ramanathan, V., & Carmichael, G. (2008). Global and regional climate changes due to black carbon. *Nature geoscience, 1*(4), 221–227. doi: 10.1038/ngeo156

Shrestha, J. N., Bajracharya, T. R., Shakya, S. R., & Giri, B. (2003). Renewable energy in Nepal-progress at a glance from 1998 to 2003. In Proceedings of the

International Conference on Renewable Energy Technology for rural Development, RETRUD-03, 12–14.

Shrestha, P. M., Chapagain, N. P., Karki, I. B., & Poudyal, K. N. (2021). Study of variability of atmospheric ozone over jumla in half period of 24 solar cycle. *Journal of Nepal Physical Society*, *7*(1), 31–38. 10.3126/jnphyssoc.v7i1.36972

Shrestha, P. M., Gupta, S. P., Adhikari, B., & Rai, K. B. (2022). Study on Seismotectonic b-value and Dc Value for Dolakha after Gorkha Earthquake 2015. *Patan Pragya*, *11*(2), 101-109, https://doi.org/10.3126/pragya.v11i02.52103

Shrestha, P. M. Gupta, S. P., Joshi, U., Rai, K. B., Chapagain, N. P., Karki, I, B., & Poudyal, K. N. (2023). Impact of Meteorological Parameters on Atmospheric Turbidity over Lumbini, Nepal, *Patan Prospective Journal*, 3(2), 104-114. https://doi.org/10.3126/ppj.v3i2.66166

Shrestha, P. M., Gupta, S. P., Rai, K. B., Joshi, U., Chapagain, N. P., Karki, I. B. & Poudyal, K. N. (2024). Comparative study of solar radiation at four sites of Nepal: A case study, *Patan Prospective Journal*, *4*(2), 79-90. https://doi.org/10.3126/ppj.v4i2.79166

Shrestha, P. M., Joshi, U., Chapagain, N. P., Karki, I. B., & Poudyal, K. N. (2020). Study of variation of aerosols on high mountain, Jomsom. *Molung Educational Frontier, 10,* 147–155. https://doi.org/10.3126/mef.v10i0.34081

Shrestha, P. M., Karki, I. B., Chapagain, N. P., & Poudyal, K. N. (2022). Atmosphericturbidity of solar radiation over Langtang national park. *Journal of Nepal Physical Society*, *8*(1), 63–69. 10.3126/jnphyssoc.v8i1.48288

Stephens, L. J., Spiegel, M. R. (1998). *Schaum's Outline of Theory and Problems of Statistics (Schaum's Outline Series)*. McGraw-Hill.

Volz, A., & Kley, D. (1988). Evaluation of the Montsouris series of ozone measurements made in the nineteenth century, *Nature, 332,* 240–242, https://doi.org/10.1038/332240a0